Magnetic properties of $Sm_3Fe_{28.1-x}Co_xMo_{0.9}$ ($x=0,4,8,12,14,16$) compounds

W. X. Li,[1,2,*] J. G. Guo,[2] B. D. Liu,[1] J. Shen,[2] G. H. Wu,[1] N. X. Chen,[2] and F. M. Yang[1]
[1]*State Key Laboratory for Magnetism, Institute of Physics, Chinese Academy of Sciences, P.O. Box 603-18, Beijing 100080, China*
[2]*Institute of Physics, University of Science and Technology Beijing, Beijing 100083, China*
(Received 17 April 2003; revised manuscript received 22 December 2003; published 27 May 2004)

A series of $Sm_3Fe_{28.1-x}Co_xMo_{0.9}$ compounds ($x=0,4,8,12,14,16$) have been synthesized and their magnetic properties and structures investigated by means of x-ray diffraction and magnetic measurements. It is found that substitution of Co for Fe leads to a significant increase of the Curie temperature and saturation magnetization. Even more important, for $x \geqslant 14$ the easy magnetization direction changes from easy plane to easy axis. In this compound system, $Sm_3Fe_{12.1}Co_{16}Mo_{0.9}$ is a very promising candidate for rare-earth permanent magnetic materials. Its room temperature saturation magnetization ($\mu_0 M_s = 1.50$ T) and anisotropy field ($B_a = 6.5$ T) are comparable to those of $Nd_2Fe_{14}B$ ($\mu_0 M_s = 1.60$ T and $B_a = 7.0$ T). However, its Curie temperature is 1020 K, which is substantially higher than that of $Nd_2Fe_{14}B$ ($T_C = 588$ K). The lattice inversion method has been employed to calculate the site occupancies of Mo and Co in the quaternary 3:29 type $Sm_3Fe_{28-x}Co_xMo$ compounds ($x=0$, 4, 8, 12, 16). The results show that Co preferentially occupies Fe1, Fe8, and Fe11 sites, whereas Mo occupies Fe3, Fe2, and Fe6 sites. As Co atoms preferentially occupy Fe1, Fe8, and Fe11 sites, the negative exchange interactions of Fe-Fe pairs associated with the sites are modified into positive and strong interactions of Fe-Co or Co-Co, which leads to the rise of Curie temperature. The bond lengths between various atoms obtained by computer simulation are used to calculate the Curie temperatures of $Sm_3Fe_{29-x}Mo_x$ ($x=0$ and 1). The calculated Curie temperature of $Sm_3Fe_{28}Mo$ is close to the experimental value.

DOI: 10.1103/PhysRevB.69.174427 PACS number(s): 75.30.Cr, 75.50.Ww, 75.40.Mg, 61.50.Ah

I. INTRODUCTION

Since the $Nd_3(Fe,Ti)_{29}$ phase[1–3] with monoclinic symmetry and space group $A2/m$ were discovered, much attention has been paid to the $R_3(Fe,M)_{29}$ compounds, where R stands for rare earth, and M for stabilizing element, such as Ti, V, Cr and Mo.[4–7] Yang *et al.*[8] and Hu *et al.*[9] have investigated the structure and magnetic properties of the $Sm_3(Fe,Ti)_{29}N_4$ compounds and found that introduction of nitrogen atoms leads to an obvious increase of the Curie temperature and saturation magnetization. Moreover, the anisotropy of the compounds changes from easy plane to easy axis upon the introduction of nitrogen atoms. These outstanding intrinsic permanent magnetic properties of the interstitial $Sm_3(Fe,Ti)_{29}N_4$ compounds make them a potential candidate for permanent magnet applications.

Later, Shah *et al.*[10] have studied the structure and magnetic properties of the $Pr_3(Fe_{1-x}Co_x)_{27.5}Ti_{1.5}$ ($x \leqslant 0.22$) compounds and found that their Curie temperature and saturation magnetization increase with Co content. Yang *et al.*[11] and Wang *et al.*[12] have investigated the structure and magnetic properties of the $Gd_3(Fe_{1-x}Co_x)_{25}Cr_4$ compounds with x ranging from 0 to 1.0 and found that when $x \geqslant 0.4$ the compounds show room temperature uniaxial anisotropy. Moreover, a higher Co content requires more Cr atoms to stabilize the 3:29 phase, and with increasing Cr content the Curie temperature and saturation magnetization increase first, going through a maximum and then decreasing. Shah *et al.* have pointed out that the large increase of T_C may result from exchange interaction enhanced by Co substitution for Fe, where there is antiparallel coupling between Fe moments. The mechanism has been supported by x-ray diffraction and later by neutron diffraction studies.[13]

In addition, Pan *et al.*[14] have studied the structure and magnetic properties of the $R_3(Fe,Mo)_{29}$ compounds and found that, compared with Cr, the required Mo content to stabilize the 3:29 phase is much smaller due to the relatively larger atomic radius of Mo. A strong advantage of choosing Mo as a stabilizing element is that the magnetic properties of the compounds are not seriously affected by the presence of the nonmagnetic Mo element.

In this paper we study the synthesis, structure, and magnetic properties of the $Sm_3Fe_{28.1-x}Co_xMo_{0.9}$ compounds ($x=0,4,8,12,14,16$). Moreover, the large increase of T_C in the compounds have been investigated by means of a new calculation based on the pair potential model,[15–17] which will be introduced in Sec. III B.

II. EXPERIMENTS

Ingots with the composition $Sm_3Fe_{28.1-x}Co_xMo_{0.9}$ ($x=0,4,8,12,14,16$) were prepared by arc melting the constituent metals with a purity of at least 99.9% under an argon atmosphere. All the ingots were melted at least four times for homogenization. To compensate for the loss of Sm during melting and annealing, an excess 30% of Sm relative to the stoichiometric composition was added. Then the ingots were sealed in a quartz tube and annealed under protection of an argon atmosphere at 1473 K for 72 h to ensure homogeneity, followed by quenching in water. X-ray diffraction (XRD) with Cu-Kα radiation and thermomagnetic analysis (TMA) were employed to identify the phases. XRD patterns for randomly oriented and normally aligned powder samples were used to determine the lattice parameters and the direction of anisotropy of the compounds, respectively. TMA was performed in a magnetic balance in a field of 0.1 T at tempera-

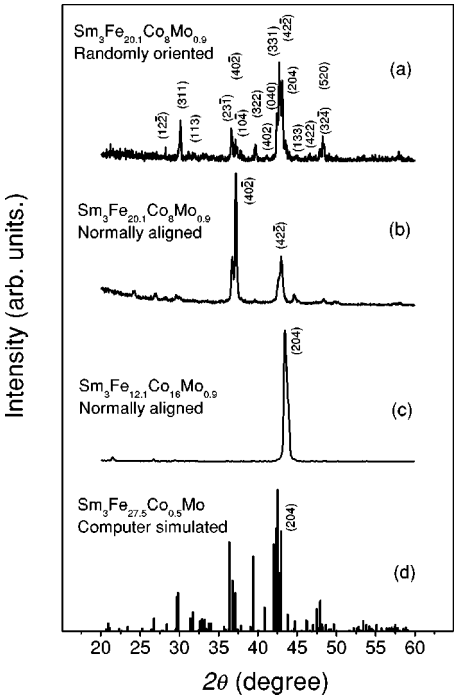

FIG. 1. XRD patterns of randomly oriented sample of $Sm_3Fe_{28.1-x}Co_xMo_{0.9}$ for $x=8$, and normally aligned samples of $Sm_3Fe_{28.1-x}Co_xMo_{0.9}$ for $x=8$ and 16. Calculated pattern of $Sm_3Fe_{27.5}Co_{0.5}Mo$.

tures ranging from room temperature to above the Curie temperature. Magnetization curves were recorded in a superconducting quantum interference device SQUID magnetometer at 5 and 293 K, respectively, in fields up to 5 T. In order to measure the anisotropy field, fine-powdered particles were mixed with epoxy resin and packed in a plastic tube of cylindrical shape. For normal magnetic alignment, the epoxy was allowed to harden while the plastic tube was positioned in an applied magnetic field of about 1 T with the cylinder axis parallel to the field direction, so that the cylinder axis becomes the easy magnetization direction (EMD). In the case of rotation alignment, the epoxy hardened while the plastic tube rotated around its cylinder axis in a magnetic field that was applied perpendicular to the axis, so that the cylinder axis will correspond to the hard magnetization direction (HMD).

III. RESULTS AND DISCUSSION

A. Crystallographic structure and magnetic properties

The XRD and TMA analyses show that the investigated compounds $Sm_3Fe_{28.1-x}Co_xMo_{0.9}$ ($x=0,4,8,12,14,16$) are single phase and crystallize in the $Nd_3(Fe,Ti)_{29}$ structure. As an example the XRD pattern of the compound $Sm_3Fe_{20.1}Co_8Mo_{0.9}$ is shown in Fig. 1(a), which is quite well indexed based on the monoclinic symmetry and space group $A2/m$. The experimental lattice constants and unit-cell volume V of the $Sm_3Fe_{28.1-x}Co_xMo_{0.9}$ compounds ($x=0$, 4, 8, 12, 14, 16) are derived from XRD patterns and listed in Table I. It can be seen that the substitution of Co for Fe leads to a decrease of the lattice constants a, b, and c as well as the unit-cell volume V, owing to smaller atomic radius of the Co atom compared with Fe.

The XRD patterns of magnetically aligned powder samples of $Sm_3Fe_{28.1-x}Co_xMo_{0.9}$ ($x=0$, 4, 8, 12, 14, 16) were measured at room temperature. As examples, the XRD patterns of normally aligned sample $Sm_3Fe_{20.1}Co_8Mo_{0.9}$ and $Sm_3Fe_{12.1}Co_{16}Mo_{0.9}$ are given in Figs. 1(b) and 1(c), respectively. It is found that, for the normally aligned powder samples, the $(40\bar{2})$ reflection for $x=8$ and (204) reflection for $x=16$ become dominant. Based on the matrix transformation relationship between the RCo_5 (1:5) structure and the monoclinic $Nd_3(Fe,Ti)_{29}$ (3:29) structure,[7] it is easy to see that the $(40\bar{2})$ and (204) reflections in $Sm_3Fe_{28.1-x}Co_xMo_{0.9}$ (3:29) correspond to the (110) and (001) reflections of the RCo_5 (1:5) structure, respectively. This suggests that the magnetocrystalline anisotropy of the compounds is of the easy-plane type for $x=8$, but of the easy-axis type for $x=16$. It is found that when x changes from 0 to 8 the anisotropy is the easy-plane type, whereas when $x=14$ and 16 the anisotropy is the easy-axis type. When $x=12$, no reflection is particularly enhanced or reduced, showing that the value of anisotropy field is about zero.

TABLE I. Comparison of the experimental (Exp.) and calculated (Cal.) parameters for $Sm_3Fe_{28.1-x}Co_xMo_{0.9}$ compounds. The calculated data are based on $Sm_3Fe_{28-x}Co_xMo$ compounds.

	$x=0$	$x=4$	$x=8$	$x=12$	$x=14$	$x=16$
Cohesive energy (eV/atom)	−4.048	−4.061	−4.074	−4.079		−4.085
a(Å)(Cal.)	10.655	10.629	10.599	10.575		10.549
b(Å)(Cal.)	8.593	8.562	8.541	8.521		8.500
c(Å)(Cal.)	9.803	9.763	9.734	9.709		9.683
β(Cal.)	96.93	97.05	97.03	97.06		97.10
V(Cal.)	890.99	881.77	874.56	868.24		861.58
a(Å)(Exp.)	10.631	10.608	10.542	10.517	10.513	10.488
b(Å)(Exp.)	8.569	8.565	8.530	8.484	8.475	8.457
c(Å)(Exp.)	9.732	9.748	9.695	9.645	9.647	9.624
β(deg)(Exp.)	96.85	96.85	96.691	96.65	96.67	96.81
V(Å^3)(Exp.)	880.50	879.39	865.93	854.82	853.90	847.67

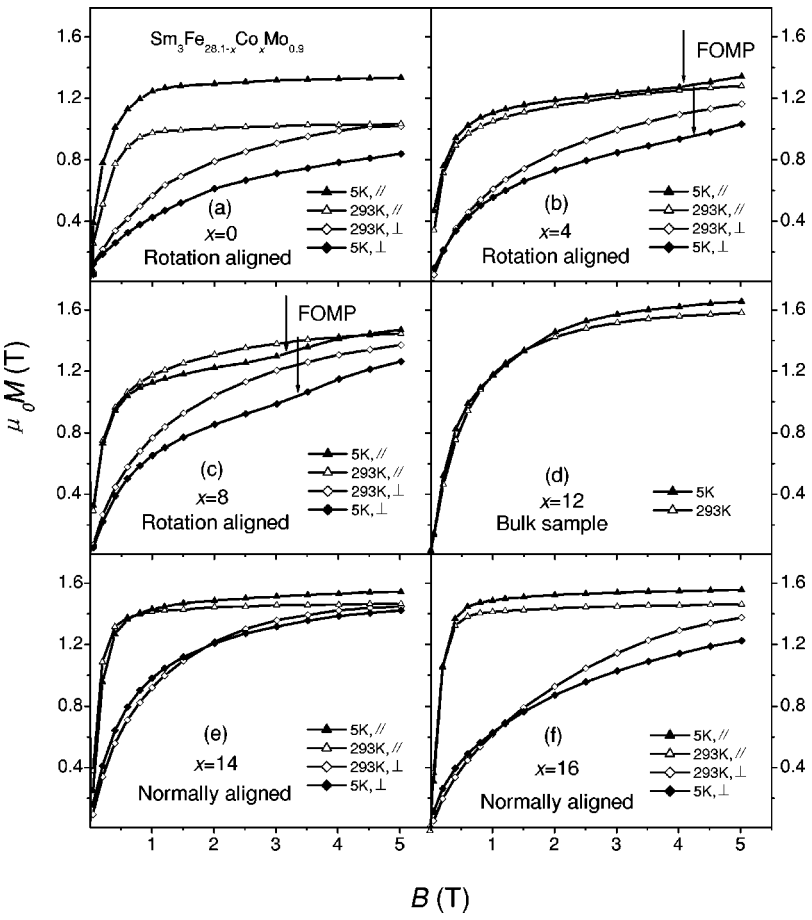

FIG. 2. Magnetization curves of $Sm_3Fe_{28.1-x}Co_xMo_{0.9}$ ($x=0,4,8,12,14,16$) compounds at 293 and 5 K.

The magnetization curves at 5 and 293 K of the $Sm_3Fe_{28.1-x}Co_xMo_{0.9}$ compounds ($x=0,4,8,12,14,16$) are shown in Fig. 2. $M_{\parallel}$ was measured with external magnetic field parallel to easy magnetization direction of the aligned samples, and $M_{\perp}$ with external magnetic field perpendicular to easy magnetization direction. The magnetocrystalline anisotropy field B_a were derived by plotting $\Delta\mu_o M$ ($\Delta\mu_o M = \mu_o M_{\parallel} - \mu_o M_{\perp}$) versus B and linearly extrapolating $\Delta\mu_o M$ to zero. Since the value of anisotropy field is about zero for $x=12$, a bulk sample was used instead to obtain the magnetization curves. The values of anisotropy field B_a are listed in Table II. It is seen that B_a reaches a value of 6.5 T for $x=16$ at room temperature.

In Figs. 2(b) and 2(c) anomalies can be found for both the easy and hard magnetization curves of $Sm_3Fe_{28.1-x}Co_xMo_{0.9}$ with $x=4$ and 8 at 5 K. The anomalies correspond to the first-order magnetization process (FOMP),[18,19] which indicates a magnetic-field-induced spin phase transition. It is also shown that the magnetization is larger at room temperature than at 5 K for $x=8$ when external field is below 4.0 T. As a result of FOMP, when external field surpasses 4.5 T, the magnetization at 5 K becomes larger than that at room temperature.

As a first-order approximation, the magnetocrystalline anisotropy contribution resulting from the rare-earth sublattice can be described by the anisotropy constant K_1^{Sm}:

$$K_1^{Sm} = -\tfrac{3}{2}\alpha_J\langle r^2\rangle\langle 3J^2 - J(J+1)\rangle A_{20}, \qquad (1)$$

where the quantities in angular brackets represent the quantum-mechanical expectation values and A_{20} is the second-order crystal-field parameter that depends on the

TABLE II. Magnetic parameters of $Sm_3Fe_{28.1-x}Co_xMo_{0.9}$ ($x=0,4,8,12,14,16$) compounds.

	$x=0$	$x=4$	$x=8$	$x=12$	$x=14$	$x=16$
EMD (293 K)	Plane	Plane	Plane	Isotropic	*c* axis	*c* axis
T_c(K)	445	665	815	920	970	1020
B_a(293 K)(T)	4.3	7.2	6.2		5.7	6.5
B_a(5 K)(T)	13.5	15.5	8.7		9.2	9.4
$\mu_0 M_s$(293 K)(T)	1.07	1.29	1.46	1.70	1.50	1.50
$\mu_0 M_s$(5 K)(T)	1.35	1.36	1.48	1.78	1.58	1.58

electrostatic potential due to the environment. Since the value of the second-order Stevens coefficient α_J is positive for Sm and the sum of the A_{20} values at the two R sites in 3:29 compounds is negative,[20] it is easily seen that the contribution of the Sm sublattice to the anisotropy is positive in 3:29 compounds. Moreover, in Fe-based ternary 3:29 compounds such as $Y_3(Fe,Ti)_{29}$,[21] the contribution of the Fe sublattice to the anisotropy is along the $[40\bar{2}]$ direction ([110] of the 1:5 structure), whereas in Co-based ternary 3:29 compounds such as $Gd_3(Co,Cr)_{29}$, the contribution of the Co sublattice is along the [204] direction ([001] direction of the 1:5 structure).[12] At a low Co content, such as when $x=0$, 4, and 8, the $Sm_3Fe_{28.1-x}Co_xMo_{0.9}$ compounds show an easy-plane type of anisotropy because the contribution of the Fe sublattice to the anisotropy is dominant. When $x=12$, the contributions of the Fe, Co, and Sm sublattices come to a balance, so that the anisotropy almost vanishes and the compound becomes nearly isotropic. With further increase of the Co content, such as for $x=14$ and 16, the contribution of the Co sublattice to the anisotropy becomes dominant, which together with contribution from the Sm sublattice, causes the compounds to exhibit easy-axis anisotropy.

The values of the saturation magnetization $\mu_o M_S$ were obtained by plotting $\mu_o M$ versus $1/B$ and extrapolating $1/B$ to zero (see Table II). With Co substitution for Fe, the value of room temperature $\mu_o M_S$ for $Sm_3Fe_{28.1-x}Co_xMo_{0.9}$ increases with Co content, going through a maximum of 1.70 T around $x=12$, then decreases with further Co content and reaches 1.50 T for $x=14$ and 16. This has been explained in terms of a rigid-band model.[22] With increasing Co content, the spin-up band of the $3d$ band of Fe is gradually filled up, so that the average magnetic moment of the $3d$ sublattice gradually increases. When the Co content increases further, the spin-up band becomes full, and the spin-down band begins to be filled up, so that the average magnetic moment of the $3d$ sublattice gradually decreases.

The temperature dependence of magnetization of the $Sm_3Fe_{28.1-x}Co_xMo_{0.9}$ compounds was measured in an applied field of 0.1 T. The Curie temperatures were derived from M^2-T curves by extrapolating M^2 to zero, as listed in Table II. With Co substitution for Fe, the Curie temperature increases monotonically from 445 K for $x=0$ to 1020 K for $x=16$. Similar to the cases for $Pr_3(Fe_{1-x}Co_x)_{27.5}Ti_{1.5}$[10] and $Nd_3(Fe_{1-x}Co_x)_{27.7}Ti_{1.3}$,[23] low Co substitution for Fe produces more rapid increase in T_C than high Co substitution. For example, an increase in T_C at 55 K per Co atom is observed for $x \leqslant 4$, compared to 25 K per Co atom in the range $12 \leqslant x \leqslant 16$.

In the $Gd_3(Fe,Co,Cr)_{29}$ compounds,[12] the amount of Cr needed for stabilization of the crystal structure is very large and also increases with Co content, which leads to a rapid decrease in the Curie temperature and saturation magnetization at high Co content. However, in the $Sm_3Fe_{28.1-x}Co_xMo_{0.9}$ compounds only a small amount of Mo is needed to stabilize the 3:29 structure, so that the magnetic properties are not seriously affected by the presence of this nonmagnetic element. Such low content of stabilizing element is responsible for obtaining the outstanding intrinsic magnetic properties at high Co content.

B. Analysis by calculations

In the $R_3(Fe,M)_{29}N_y$ compounds such as $Sm_3(Fe,M)_{29}N_4$,[8] the introduction of interstitial nitrogen atoms leads to an expansion of the lattice, which results in increase of the Curie temperature. However, in the $R_3(Fe,Co,M)_{29}$ compounds, with Co substitution for Fe the unit-cell volume usually decreases whereas the Curie temperature increases,[10,23] so the increase of T_C in $R_3(Fe,Co,M)_{29}$ compounds can not be explained by lattice expansion.

According to the viewpoint of Givord *et al.*[24] and Gavigan *et al.*,[25] in Fe-rich *R*-Fe interatomic compounds, there is a positive exchange interaction when the bond length between Fe atoms is larger than 2.45 Å, and a negative exchange interaction where the bond length is smaller than 2.45 Å. In addition, it is found that the exchange interactions of the Co-Co (or Co-Fe) pairs are larger than those of Fe-Fe pairs in $Y(Fe,Co)_{10}Si_2$. This is because no exchange interactions exist between Co-Co bond and Co-Fe bonds but between Co-Co moments (or between Co-Fe moments).[26] This may also be true in the $Sm_3Fe_{28.1-x}Co_xMo_{0.9}$ compounds. Therefore, it is acceptable that the increase in T_C upon the substitution of Co for Fe, especially in low Co substitution, may be explained by the preferential occupancy of Co atoms, modifying the negative exchange interactions of Fe-Fe pairs into positive and strong interactions of Fe-Co or Co-Co. Such an explanation is applicable to many Co-substituted *R*-Fe compounds, such as $R_2Fe_{14-x}Co_xB$,[27] $DyFe_{10-x}Co_xV_2$,[28] and $Pr_3(Fe_{1-x}Co_x)_{27.5}Ti_{1.5}$.[10]

Using the method of Rietveld analysis, Shah *et al.*[10] obtained all the bond lengths between the $3d$ sites in $Pr_3(Fe_{1-x}Co_x)_{27.5}Ti_{1.5}$ compounds and proposed that Co atoms might preferentially occupy Fe1 and Fe8 sites associated with negative interactions. If Co atoms occupy either of these two sites, a large increase in T_C can be expected. Harris *et al.*[13] carried out neutron diffraction studies in $Pr_3(Fe_{1-x}Co_x)_{27.5}Ti_{1.5}$ at low Co content and indicated that Ti atoms occupy $4g$ and $4i$ sites. However, the neutron diffraction refinement analysis, although in accordance with the mechanism of increase in T_C proposed by Shah *et al.*, shows that Co atoms occupy, without preference, these Fe sites not shared with Ti atoms. Here, we should mention that the nomination of Fe sites in Ref. 13 is different from that in this paper and in Ref. 10. However, from the atom position and site symmetry, one can find that the sites Fe1, Fe2, Fe3, Fe4, Fe5, Fe6, Fe7, Fe8, Fe9, Fe10, and Fe11 in Ref. 13 correspond to Fe1, Fe11, Fe6, Fe7, Fe9, Fe3, Fe2, Fe5, Fe4, Fe10, and Fe8 in Ref. 10, respectively.

To investigate the site preference of Co and Mo, establish a detailed distribution of the Fe-Fe negative interaction bonds with various Co content, and then investigate the increase in the Curie temperature of the quaternary $Sm_3(Fe,Co,Mo)_{29}$ compounds, computer simulation studies have been performed by the lattice inversion method. A whole calculation process would involve the following steps: at first, the cohesive energy $E(x)$ can be obtained by either

the first-principle calculation or experimental data; then, all the intermetallic potentials $\Phi(x)$ can be deduced based on lattice inversion method (Sec. III B 1); next, based on the structure and space group, the preferential occupancy of atoms, the lattice parameters, and the distance of every atomic pair can be calculated (Sec. III B 2 and 3); finally, these calculated distances are used to investigate the Curie temperature (Sec. III B 3).

1. Lattice inversion method

In principle, any interatomic pair potential can be obtained by a strict lattice inversion of cohesive energy curves. In this paper, acting on the lattice inversion method developed by Chen,[15–17] we can avoid parameter adjustment when deriving the interatomic potentials. The method can be summarized as follows: it assumes that cohesive energy per atom in a perfect crystal can be expressed as the sum of pair potentials, i.e.,

$$E(x)=\frac{1}{2}\sum_{n=1}^{\infty} r_0(n)\Phi[b_0(n)x], \tag{2}$$

where x is the nearest-neighbor distance, $r_0(n)$ is the nth neighbor coordination number, $\Phi(x)$ is the pair potential function and $b_0(n)x$ is the distance of the nth neighbor from the reference atom, with $b_0(1)=1$. We extend the series $\{b_0(n)x\}$ to a multiplicative closed semigroup $\{b(n)x\}$, in which, for any two integers m and n , there exists an integer k so that $b(k)=b(m)b(n)$. Thus

$$E(x)=\frac{1}{2}\sum_{n=1}^{\infty} r(n)\Phi[b(n)x], \tag{3}$$

where

$$r(n)=\begin{cases} r_0(b^{-1}[b(n)]), & b(n)\in\{b_0(n)\}, \\ 0, & b(n)\notin\{b_0(n)\}. \end{cases} \tag{4}$$

In the above extension, we have to insert some virtual lattice point in $r(n)$. Then the pair potential $\Phi(x)$ can be obtained:

$$\Phi(x)=2\sum_{n=1}^{\infty} I(n)E[b(n)x], \tag{5}$$

where the inversion coefficient $I(n)$ is given by

$$\sum_{b(n)|b(k)} I(n)r\left\{b^{-1}\left(\frac{b(k)}{b(n)}\right)\right\}=\delta_{k1}, \tag{6}$$

which is uniquely determined by the crystal geometrical structure, irrespective of the atomic species. Thus the intermetallic pair potentials between identical atoms like $\Phi_{Fe-Fe}(x)$ can be deduced if the cohesive energy $E(x)$ has been obtained. For a concise description of the whole calculation process, the acquisition of cohesive energy $E(x)$ and the intermetallic pair potentials between distinct atoms such as $\Phi_{Fe-Co}(x)$, as well as the transferability of intermetallic pair potentials are introduced in the Appendix.

2. Atomic preferential occupancy

Based on any existing experimental structure close to $Nd_3(Fe,Ti)_{29}$ type with the $A2/m$ space group, for example, the atom position and symmetry of Ref. 7, initial Sm_3T_{29} structure is constructed within Accelrys Cerius 2 modeling software. The assignment of Fe sites in this paper is in accordance with Ref. 10. To reduce statistical fluctuations, a periodic cell $[(Sm_3T_{29})_2]_{2\times2\times2}$ containing $2\times2\times2\times64$ atoms is taken as a calculation unit. The conjugate gradient method is adopted for energy minimization with a cut-off radius of 14 Å. Once the energy minimization process based on the intermetallic pair potential is carried out, the somehow arbitrary initial structure will reach a stabilized structure with minimized cohesive energy, provided that the initial model does not deviate too much from the existing $Nd_3(Fe,Ti)_{29}$ type structure. All these configurations are relaxed, and the energy and lattice parameters are averaged over 20 sample units. The randomness of initial structure in a certain range and the stability of the final structure furnish convincing evidence that the interatomic pair potentials are reliable for the study of structural properties of materials.

Compared with ternary systems, the substitution in a quaternary system is more complex since there may exist competition when more than one element is added. Therefore, at first we use the hypothetical model of Sm_3Co_{29}, Sm_3Fe_{29}, $Sm_3Co_{28.5}Mo_{0.5}$, $Sm_3Fe_{28.5}Mo_{0.5}$ and $Sm_3Fe_{28.5}Co_{0.5}$ with the $A2/m$ space group to investigate the substitution behavior of the elements Mo and Co. All the foreign atoms are supposed to be induced to one of the 11 Fe sites to substitute for the original atoms, and the cohesive energy is adopted as a criterion for site preference. Figures 3(a) and 3(b) show the preferential sites of Mo and Co in the $Sm_3(Fe,Co,Mo)_{29}$. It can be seen that the Mo atom has the same site preference in Co-based as in Fe-based compounds, and the preferential sites are Fe3 ($4i$), Fe2 ($4i$), and Fe6 ($4g$). With the Mo substitution for Fe or Co, the cohesive energy declines dramatically for all the 11 Fe sites, which indicates that Mo strongly stabilizes the metastable Sm_3T_{29} structure. Interestingly, the graphs of Figs. 3(a) and 3(c) are asymmetric, which shows the preferential occupancy of Co and Mo are totally different for these 11 Fe sites. It is shown in Fig. 3(c) that with Co substitution for Fe, the 11 sites of Sm_3T_{29} structure fall into 3 groups. Co substitution for Fe does not lead to as much energy decline as Mo; on the contrary, it leads to an increase in cohesive energy in Fe3 ($4i$), Fe2 ($4i$), and Fe6 ($4g$). The most unfavorable sites Fe3 ($4i$), Fe2 ($4i$), and Fe6 ($4g$) for Co, are just the preferential sites for Mo, whereas the preferential sites for Co are Fe1 ($2c$), Fe8 ($8j$), and Fe11 ($4e$), which are just the unfavorable sites for Mo. The other five sites, with almost the same energy decline, are the second-favorable sites for Co.

In light of the above discussion, in order to study the Co substitution behavior in the quaternary system it is reasonable to preset Mo in Fe3 ($4i$), Fe2 ($4i$), and Fe6 ($4g$) sites for their strong site preference. Considering the little difference in site preference of these three sites, we preset the same fractional occupancy for Mo occupancies of 16.7% in each of these three sites. Then Co atom is induced to substitute Fe in one of the 11 sites. Once the energy minimization

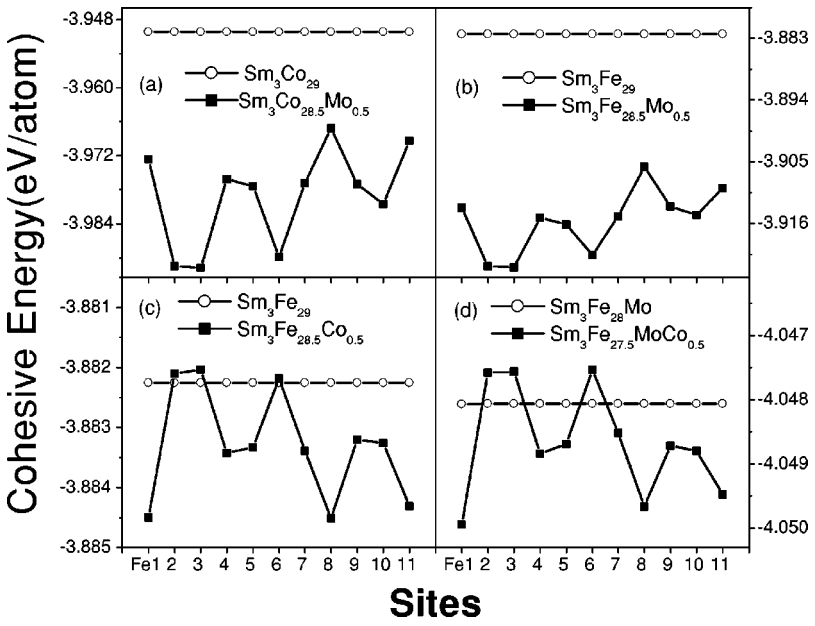

FIG. 3. Site preference of Mo and Co in $Sm_3(Fe,Co,Mo)_{29}$ compounds.

is applied to relax the quaternary system under the interaction of pair potentials, the relaxed structure can still retain the Sm_3T_{29} structure with the $A2/m$ space group [see Fig. 1(d)]. Furthermore, by comparing Fig. 3(c) with Fig. 3(d), it is shown that Co has the same site preference in $Sm_3Fe_{27.5}MoCo_{0.5}$ as in $Sm_3Fe_{28.5}Co_{0.5}$.

The calculated results of Mo preferential occupancy in Fe3, Fe2, and Fe6 sites coincide well with XRD and neutron diffraction studies.[6,10,13] As for the Co site preference, the preferential sites in our calculation are Fe1, Fe8, and Fe11 sites, which are similar to Fe1 and Fe8 sites proposed by Shah *et al.*[10] In addition, both the calculation and the neutron-diffraction studies by Harris *et al.*[13] agree that Fe3, Fe2, and Fe6 sites are the unfavorable sites for Co substitution.[13] However, for Co substitution, all the 11 sites fall into 3 groups in our calculation, compared to the neutron-diffraction results: Co atoms occupy without preference in the eight Fe sites other than Fe3, Fe2, and Fe6 sites.[13] The precision of pair potentials can be one of sources to bring difference in Co occupancy between the calculation and the neutron-diffraction studies. Furthermore, the presence of a residual α-Fe phase of 9 wt% in neutron-diffraction sample and the details of refinement analysis can influence the accuracy of the fractional occupancy. Thus, single-phase samples especially at high Co content, are required to investigate Co substitution behaviors in 3:29 compounds by neutron-diffraction studies.

We further simulate the quaternary system $Sm_3Fe_{28-x}MoCo_x$ with higher Co concentration ($x=4$, 8, 12, 16). For all the Co composition, Mo occupancy is preset to be 16.7% in each of Fe3, Fe2, and Fe6 sites, with no Co atoms occupancy in these sites. For low substitution such as $x=4$, all Co atoms are added to Fe1, Fe8, and Fe11 sites with the same factional occupancy at 57.1%. For higher substitution such as $x=8$, 12, and 16, the favorable sites (Fe1, Fe8, and Fe11) are assumed to be completely occupied by Co atoms, and excess Co atoms are induced to the second-favorable sites (Fe4, Fe5, Fe7, Fe9, and Fe10) with Co occupancy at 0.63% for $x=8$, at 31.3% for $x=12$ and at 56.3% for $x=16$ in each of these second-favorable sites. The calculation results show that with increasing Co content the cohesive energy decreases gradually (see Table I). The calculated lattice parameters and cohesive energy at different Co content are listed in Table I. The differences in lattice parameter between experiment and calculation always fall within 1%.

As a practical approximation, the favorable sites are assumed to be completely occupied by Co atoms for high Co substitution. This assumption is based on the calculated results of Co site preference, since there are no reports for high Co substitution behaviors in 3:29 compounds by neutron diffraction studies. The cases of mixed occupancy in the sites (more than two elements in a certain site), probably useful to improve the precision in calculation, are not taken into consideration due to the complicated calculation process.

3. Interatomic distance and Curie temperature

As mentioned above, in ternary or quaternary systems such as $Sm_3(Fe,Co,Mo)_{29}$, a $3d$ site may be occupied by either an Fe, Co, or Mo atom, so the distances between two $3d$ sites will be different for different $3d$ atoms. Based on the computer simulation, the bond length between any atomic pair and the number of neighboring atoms for each atom have been obtained. For simplicity, only the bond lengths between Fe-Fe sites in a crystal cell are listed in Table III. For $x=0$, the bonds with length shorter than the critical value of 2.45 Å are Fe2-Fe3, Fe4-Fe8, Fe6-Fe6, and Fe8-Fe11 bonds, compared to Fe1-Fe5, Fe2-Fe3, Fe4-Fe8, and Fe8-Fe11 bonds in the x-rays Rietveld analysis results of $Pr_3(Fe_{1-x}Co_x)_{27.5}Ti_{1.5}$.[10] With the substitution of Co for Fe, additional Fe-Fe bonds become available for negative interaction. These bonds in the calculation are Fe7-Fe8 for $x=4$ and $x=8$, Fe7-Fe8 and Fe1-Fe5 for $x=12$, and Fe7-Fe8, Fe1-Fe5, and Fe4-Fe5 for $x=16$. For both the calculation and the x-rays Rietveld analysis, Fe7-Fe8 is always considered as the bond available for negative interaction upon Co

TABLE III. Calculated bond lengths between Fe-Fe sites in Å for $Sm_3Fe_{28-x}Co_xMo$ compounds.

Bond type	$x=0$	$x=4$	$x=8$	$x=12$	$x=16$
Sm1-Fe2×2	3.041	3.036	3.027	3.024	3.000
Fe4×4	3.052	3.018	3.005	2.998	3.011
Fe6×2	3.094	3.080	3.072	3.059	3.056
Fe7×2	2.953	2.945	2.976	2.958	2.957
Fe9×2	3.045	3.037	3.036	3.039	2.938
Sm2-Fe3×1	3.057	3.044	3.042	3.029	3.017
Fe4×2	3.100	3.099	3.090	3.083	3.045
Fe5×4	3.049	3.043	3.036	3.031	3.037
Fe7×1	3.036	3.021	3.044	3.025	3.034
Fe9×1	3.011	3.013	3.003	2.988	2.990
Fe10×2	2.971	2.986	3.001	2.991	2.966
Fe1-Fe3×2	2.589	2.617	2.621	2.608	2.604
Fe5×4	2.465	2.464	2.460	2.429	2.435
Fe10×4	2.490	2.474	2.470	2.471	2.465
Fe2-Fe3×1	2.439	2.441	2.455	2.444	2.436
Fe4×2	2.755	2.761	2.752	2.763	2.746
Fe5×2	2.799	2.801	2.786	2.761	2.725
Fe6×2	2.903	2.882	2.892	2.885	2.893
Fe8×2	2.681	2.557	2.590	2.646	2.638
Fe9×1	2.829	2.803	2.761	2.773	2.759
Fe11×2	2.625	2.534	2.548	2.545	2.599
Fe3-Fe4×2	2.743	2.737	2.730	2.729	2.736
Fe5×2	2.818	2.818	2.823	2.804	2.784
Fe6×2	2.958	2.937	2.946	2.949	2.951
Fe7×1	2.700	2.680	2.652	2.658	2.658
Fe8×2	2.568	2.531	2.555	2550	2537
Fe10×2	2.783	2.773	2.738	2.679	2.728
Fe4-Fe5×1	2.493	2.489	2.480	2.476	2.444
Fe6×1	2.733	2.718	2.681	2.706	2.685
Fe7×1	2.561	2.562	2.566	2.565	2.544
Fe8×1	2.542	2.532	2.526	2.509	2502
Fe8×1	2.401	2.396	2.398	2.398	2.381
Fe9×1	2.564	2.564	2.572	2.550	2.538
Fe10×1	2.672	2.659	2.656	2.629	2.624
Fe11×1	2.483	2.476	2.476	2.469	2.453
Fe5-Fe5×1	2.511	2.510	2.498	2.491	2.485
Fe8×1	2.486	2.472	2.475	2.467	2.462
Fe9×1	2.652	2.640	2.658	2.640	2.647
Fe10×2	2.560	2.547	2.558	2553	2.704
Fe10×1	2.673	2.670	2.688	2.685	2.539
Fe6-Fe6×1	2.417	2.419	2.421	2.416	2.410
Fe7×2	2.683	2.685	2.698	2.706	2.709
Fe8×2	2.603	2.598	2.581	2.574	2.568
Fe11×2	2.564	2.570	2.576	2.572	2.569
Fe7-Fe8×2	2.451	2.449	2.449	2.449	2.447
Fe11×2	2.458	2.451	2.461	2.464	2.476
Fe8-Fe9×1	2.503	2.493	2.490	2.487	2.487
Fe10×1	2.501	2.479	2.490	2.468	2.474
Fe11×1	2.394	2.380	2.374	2.370	2.374
Fe9-Fe10×2	2.482	2.492	2.507	2.482	2.469
Fe10-Fe10×1	2.483	2.486	2.505	2.488	2.483

TABLE IV. Number of the bond lengths shorter than 2.45 Å in $2\times2\times2$ crystal cells for $Sm_3Fe_{28-x}Co_xMo$ compounds.

	$x=0$	$x=4$	$x=8$	$x=12$	$x=16$
$3d$-$3d$(total)	107	146	176	203	265
Co-Co	0	13	59	66	95
Co-Fe	0	81	91	121	158
Mo-3d	0	0	0	0	0
Fe-Fe	107	52	26	16	12
Fe-Fe%	100	35.62	14.77	7.88	4.53

substitution. Small difference in bond length between the calculation and the x-rays Rietveld analysis can result from many sources, including the precision of pair potentials, the assumption to distribute Co or Mo atoms equally on each of the preferential sites, and the details of refinement analysis, for example, Co was omitted for the XRD refinement due to the inability of x rays to differentiate between Co and Fe.[10,13]

The numbers of all the bond lengths shorter than 2.45 Å between $3d$ atoms in a calculation unit of $2\times2\times2$ crystal cells (512 atoms in total) are listed in Table IV. Since Mo atoms occupy Fe3 $(4i)$, Fe2 $(4i)$, and Fe6 $(4g)$ sites, no Mo atom is found to associate with the bonds shorter than 2.45 Å. It can be seen that with increasing Co content, the total number of bonds between $3d$ atoms with length shorter than the critical value 2.45 Å increases, including Fe-Co and Co-Co bonds. However, the Fe-Fe bonds available for negative interaction decrease drastically. Figure 4 shows the Co composition dependence of the lattice parameter *a*, the number of Fe-Fe bonds available for negative interaction and the Curie temperature T_C. From Fig. 4 and Table IV, the computer simulation proves that as Co atoms preferentially occupy on certain sites, the negative exchange interactions of Fe-Fe pairs associated with the sites are modified into positive and strong interactions of Fe-Co or Co-Co. Thus, the Curie temperature is greatly elevated, especially in low Co substitution.

Since the interatomic bonds for all the neighboring atoms in 3:29 compounds can be determined through computer simulation, the bond lengths obtained can be applied to calculate the Curie temperature in the $Sm_3Fe_{29-x}Mo_x$ compounds. Li *et al.*[29–31] investigated the systems of $Nd_2Fe_{14}B$, Sm_2Fe_{17}, and $Sm_2Fe_{17-x}Si_x$ by ^{57}Fe Mössbauer spectra. In the compound Sm_2Fe_{17}, the exchange integrals as a function of distance between the Fe-Fe bonds were obtained by fitting the hyperfine field data at various temperatures for each Fe site. However, due to the difficulty in managing the Fe-Fe bonds with various distances, all the integrals were assumed to fall into two groups. The positive exchange integrals were taken with $J_+=55$ K on the average and the negative exchange integrals were taken with $J_-=-115$ K on the average.

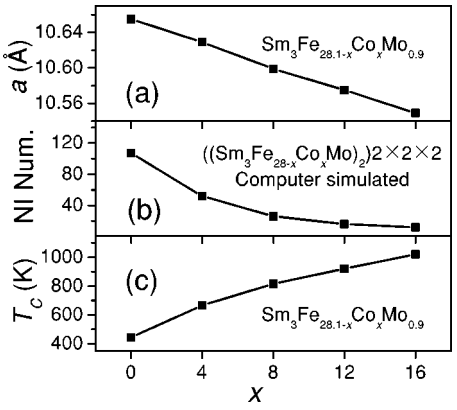

FIG. 4. Co composition dependence of lattice parameter *a*, number of Fe-Fe bonds available for negative interaction, and Curie temperature.

However, with the detailed data obtained for any bond between $3d$ atoms, there is no need to distinguish an Fe-Fe bond by distance in the computer calculation. In the $Sm_3Fe_{29-x}Mo_x$ compounds, all the Fe atoms in the calculated unit are marked by *p*, if the contribution to Curie temperature of the low concentration of Mo can be neglected. The neighboring atom *q* is confined to the Fe atom with bond length shorter than 3.15 Å to a given *p* atom. According to the theory of molecular fields, the contribution of Fe-Fe exchange interaction to the Curie temperature, T_{Fe-Fe} is simply given by

$$T_{Fe-Fe}=\frac{2S(S+1)}{3}\frac{1}{P}\sum_{p=1}^{p}\sum_{q=1}^{Z_p}J_{pq}, \tag{7}$$

where J_{pq} is the exchange integral between the *p* and *q* atoms, Z_p is the number of the neighboring *q* atoms to a given *p* atom, *S* is the spin quantum number taken to be 1 for Fe, and *P* is the total number of Fe atoms in the calculated unit. For a periodic cell $[(Sm_3Fe_{29})_2]_{2\times2\times2}$, *P* is 464, and for $[(Sm_3Fe_{28}Mo)_2]_{2\times2\times2}$, *P* is 448. Since no exact data of exchange integrals as a function of distances between the Fe-Fe bonds is available for the 3:29 compound in the literature, the data for Sm_2Fe_{17} were taken instead to calculate the Curie temperature.[31] Then the calculated value of T_{Fe-Fe} for Sm_3Fe_{29} is 337 K, while for $Sm_3Fe_{28}Mo$ it is 332 K. With Mo substitution for 1/29th of the Fe atoms in the Sm_3Fe_{29} compound, the Curie temperature merely decreases by 5 K. By analysis of the calculated data for bond length, it shows that although the total number of Fe-Fe bonds decreases with the Mo substitution for Fe in Sm_3Fe_{29}, the Fe-Fe exchange integral on the average still increases as a result of the increase of cell parameters and bond lengths on the average. In addition, it is found in our calculation that among all the Fe-Fe bond lengths for $Sm_3Fe_{28}Mo$, only 23% of bond lengths are larger than 2.70 Å, and only 26% for Sm_3Fe_{29}. However, among all the Mo-Fe and Mo-Mo bond lengths for $Sm_3Fe_{28}Mo$, 80% of bond lengths are larger than 2.70 Å, and for the original Sm_3Fe_{29}, 60% of the corresponding Fe-Fe bond lengths associated with Mo substitution for Fe are larger than 2.70 Å. In light of the above discussion, we can conclude that Mo atoms not only preferentially occupy Fe3$(4i)$, Fe2$(4i)$, and Fe6$(4g)$ sites, but also preferentially displace the Fe atoms associated with bond lengths larger than 2.70 Å. The literature shows that when the bond lengths are larger than 2.70 Å, the Fe-Fe exchange integral $J_{Fe\text{-}Fe}$ becomes very small and contributes little to the Curie

temperature.[31] Thus, with low concentration of Mo substitution for Fe, both the total-exchange interactions and the Curie temperature of the compound will not decrease notably.

Among Mo, Fe, and Co, the atomic radius of Mo is the largest and that of Co is the smallest. The calculation shows that Mo atoms preferentially replace the Fe atoms associated with larger bond length, and Co atoms preferentially replace the Fe atoms associated with smaller bond length. From this size-effect, it is acceptable for our assumption that all the 11 Fe sites in 3:29 compounds would fall into 3 groups as for Co (Mo) substitution for Fe. It is worth noting that the results of Co (Mo) site preference based on cohesive energy criterion can be well understood by the size effect.

It is well known that in the *R*-*T* compounds T_C is mainly determined by the *T*-*T* exchange interaction, and the *R*-*R* exchange interaction can be neglected. However, the contribution of the *R*-Fe exchange interaction to the Curie temperature should be considered. Hence, for $Sm_3Fe_{29-x}Mo_x$, the Curie temperature can be expressed as

$$T_C=\frac{2S(S+1)}{3}\frac{1}{P}\sum_{p=1}^{p}\sum_{q=1}^{Z_p}J_{pq}+T_{Sm-Fe}. \tag{8}$$

The Curie temperatures for $Sm_3Fe_{28.1}Mo_{0.9}$ and $Y_3Fe_{28.1}Mo_{0.9}$ are 445 and 376 K,[32] respectively. Since $T_{Y\text{-}Fe}$ is zero, the contribution of the Sm-Fe exchange interaction to the Curie temperature, $T_{Sm\text{-}Fe}$, can be estimated to be about 69 K. Thus, the calculated Curie temperature is 406 K for Sm_3Fe_{29} and 401 K for $Sm_3Fe_{28}Mo$. The latter is close to the experimental value of 445 K for $Sm_3Fe_{28.1}Mo_{0.9}$. The calculated result is appreciably smaller than the experimental result, which may result from the difference of $J_{Fe\text{-}Fe}$ between 3:29 compounds and 2:17 compounds. Mössbauer spectra studies, therefore, are required to obtain the exchange integrals $J_{Fe\text{-}Fe}$ as a function of distance in 3:29 compounds for a more accurate calculation of Curie temperature. In addition, if the exchange integrals $J_{Fe\text{-}Co}$ and $J_{Co\text{-}Co}$ as a function of distance can be found, Eq. (8) may be used to calculate the Curie temperature of $Sm_3Fe_{28-x}Co_xMo$ compounds.

IV. CONCLUSION

In summary, the $Sm_3Fe_{28.1-x}Co_xMo_{0.9}$ compounds with $x=0,4,8,12,14,16$ crystallize in the $Nd_3(Fe,Ti)_{29}$ type structure with monoclinic symmetry and space group $A2/m$. Substitution of Co for Fe leads to a significant increase of the Curie temperature and saturation magnetization. Even more important, for $x\geqslant 14$ the easy magnetization direction changes from easy plane to easy axis. In this compound system, the room-temperature saturation magnetization ($\mu_o M_S=1.50$ T) and anisotropy field ($B_a=6.5$ T) of $Sm_3Fe_{12.1}Co_{16}Mo_{0.9}$ are comparable to those of $Nd_2Fe_{14}B$ ($\mu_o M_S=1.60$ T and $B_a=7.0$ T), but the Curie temperature is 1020 K, which is substantially higher than that of $Nd_2Fe_{14}B$ ($T_C=588$ K), showing favorable intrinsic permanent magnetic properties as a promising candidate for permanent-magnet applications. Based on the lattice inversion method, the site occupancies of Mo and Co in the quaternary $Sm_3Fe_{28-x}Co_xMo$ compounds have been performed by computer simulation. It is found that Mo atoms, with larger atomic radius compared with Co and Fe, not only preferentially occupy Fe3 ($4i$), Fe2 ($4i$), and Fe6 ($4g$) sites, but also preferentially substitute the Fe atoms associated with larger bond length and less contribution to the total exchange interaction. Thus, the Curie temperature of the compound will not decrease notably upon the Mo substitution. While the Co atoms, with smaller atomic radius compared with Fe and Mo, preferentially occupy Fe1 ($2c$), Fe8 ($8j$), and Fe11 ($4e$) sites, modifying the negative exchange interactions of Fe-Fe pairs into positive and strong interactions of Fe-Co or Co-Co. Thus, the Curie temperature is greatly elevated especially in low Co substitution. Finally, based on the bond lengths between various atoms obtained by computer simulation, the Curie temperatures for $Sm_3Fe_{28}Mo_x$ ($x=0$ and 1) compounds have been calculated.

ACKNOWLEDGMENT

This work was supported by the State Key Program for Fundamental Research in China under Grant No. G2000067106.

APPENDIX

1. Total-energy calculations and parameter fitting

The cohesive energy curves for pure metals and some ordered alloys with simple structure can be obtained by either the first principle calculation or experimental data.

For the first principle calculation, cohesive energy $E(x)$ is defined as

$$E(x)=E_{tot}(x)-E_{tot}(\infty), \tag{A1}$$

where x is the nearest-neighbor distance, $E_{tot}(x)$ the total energy, and $E_{tot}(\infty)$ the energy for isolated atoms. The total energies are calculated based on the Generalized Gradient Approximation (GGA) density functional theory with the ultrasoft pseudopotentials.[33,34]

For simplicity, the equation with Rose form

$$E(x)=-E_0[1+\beta(x-x_0)]e^{-\beta(x-x_0)}, \tag{A2}$$

is used to fit the binding energy curve $E(x)$, where E_0 is the sublimation energy, and x_0 the equilibrium nearest-neighbor distance, with

$$\beta=\left(\frac{9B\Omega_0}{x_0^2E_0}\right)^{1/2}, \tag{A3}$$

where B is the bulk modulus and Ω_0 the equilibrium atomic volume. Thereby, these parameters E_0, B, and Ω_0 can be obtained by fitting the calculated cohesive energy curves according to above equation.

Alternatively, the cohesive curves can be directly determined if the experimental data E_0, B, and Ω_0 are available in literature. In this work, the cohesive energy curves between identical atoms are obtained from the experimental data. Those between distinct atoms are obtained from fitting the first-principles calculation results owing to the difficulty to find corresponding experimental data.

2. Intermetallic pair potentials between distinct atoms

At first, the intermetallic pair potential between identical atoms can be calculated based on the formulas in Sec. III B 1 and the cohesive energy obtained.

Then, by assuming the transferability of these potentials from simple structure FCC or BCC metals to other intermetallic compounds,[35] the binding energy $E_{A-B}(x)$ contributed by the cross interactions in a compound $A_{y_A}B_{y_B}$ can be formulated as

$$E_{A-B}(x)=E(x)-\frac{y_A}{2}\sum_{\mathbf{R}_A\neq 0}\Phi_{A-A}(|\mathbf{R}_A|)$$

$$-\frac{y_B}{2}\sum_{\mathbf{R}_B\neq 0}\Phi_{B-B}(|\mathbf{R}_B|), \tag{A4}$$

where y_A (y_B) is the atomic composition, $\mathbf{R}_A$ ($\mathbf{R}_B$) the position vector of an A-type (B-type) atom, and $E(x)$ the equation of state of the parent compound. The sums are over all the A-type (B-type) atoms with origin at one of A (B) atoms, respectively. $E_{A-B}(x)$ can also be expressed as

$$E_{A-B}(x)=y_A\sum_{\mathbf{R}_B\neq 0}\Phi_{A-B}(|\mathbf{R}_B|), \tag{A5}$$

where Φ_{A-B} is the potential between atoms A and B. The sum is over all the B atoms but with origin at one of A atoms. Note Eq. (A5) is equivalent to Eq. 2, Φ_{A-B} can be obtained from $E_{A-B}(x)$ by using Eqs. (5), (A4), and (A5). All the interatomic potentials between distinct atoms as well as these between identical atoms have been plotted in Fig. 5.

3. Assumption of the transferability of intermetallic pair potentials

It is true that the intermetallic pair potential and the cohesive energy are related to the various neighbor-atom configurations for multielement systems, thus the pair potential and the cohesive energy would not be the same after the Mo or Co substitution for Fe in 3:29 compounds. But most of the atomistic simulation methods for complex systems are unfortunately quite complicated and time consuming especially when there are too many adjustment parameters in the calculations.

In our semiempirical simulation based on lattice inversion method, as a practical approximation, the intermetallic pair potential obtained from simple structures such as FCC and BCC are assumed to be able to transfer to other complex intermetallic structures without any adjustment parameter. We can thereby simulate the multielement system with large cell, e.g., $[(Sm_3Fe_{28-x}MoCo_x)_2]_{2\times 2\times 2}$ in this paper, and take the relaxation effect into account, sheering away the difficulties of quantum mechanics when treating large cell.

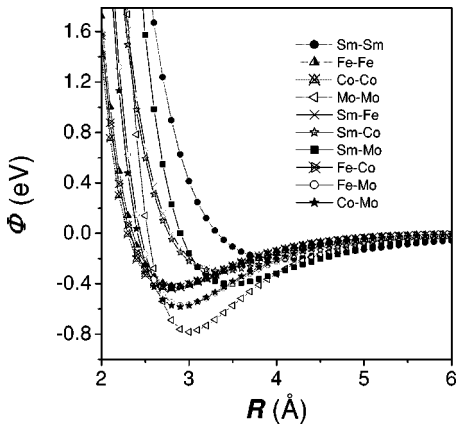

FIG. 5. Pair potentials in $Sm_3(Fe,Co,Mo)_{29}$ compounds.

The validity of the transferability of intermetallic pair potentials has been supported by our previous work. The intermetallic pair potentials have been successfully applied to reproduce cohesive energy, bulk modulus, phonon spectrum, and some other simple properties very well. In particular, the inverted potentials are found to be quite effective for the calculations of structural properties such as lattice parameter and site preference in rare-earth intermetallic compounds.[36–39] In addition, the small difference between the pair potentials Φ_{A-B} inverted from different superstructures also provides evidence for transferring pair potentials from one structure to another.[35]

However, the intermetallic pair potentials based on the lattice inversion method are not universal for any atomistic simulation. When dealing with the ion crystal such as NaCl,[40] coulomb interaction has been considered to modify the inverted pair potentials. What is more, the intermetallic pair potentials are ineffective to calculate the compounds with strong orientation. Considering the contribution of the covalent bond in semiconductor, Liu *et al.*[41] have applied three-body potentials to describe semiconductor, despite a time-consuming convergence process in this case.

*Email address: leewx@aphy.iphy.ac.cn

[1] S.J. Collocott, R.K. Day, J.B. Dunlop, and R.L. Davis, in *Proceedings of 7th International Symposium on Magnetic Anisotropy and Coercivity in Rare Earth-Transition Metal Alloys* (Canberra, 1992), p. 437.

[2] H.S. Li, J.M. Cadogan, R.L. Davis, A. Margarian, and J.B. Dunlop, Solid State Commun. **90**, 487 (1994).

[3] O. Kalogirou, V. Psycharis, L. Saettas, and D.N. Niarchos, J. Magn. Magn. Mater. **146**, 335 (1995).

[4] M.R. Ibarra, L. Morellon, J. Blasco, L. Pareti, P.A. Algarabel, J. Garcia, F. Albertini, and A. Paoluzzi, J. Phys.: Condens. Matter **6**, L771 (1994).

[5] C.D. Fuerst, F.E. Pinkerton, and J.F. Herbst, J. Appl. Phys. **76**, 6144 (1994).

[6] Q.L. Liu, G.H. Rao, J.K. Liang, and B.G. Shen, J. Appl. Phys. **88**, 4241 (2000).

[7] X.F. Han, H.G. Pan, H.L. Liu, F.M. Yang, and Y.W. Zheng, Phys. Rev. B **56**, 8867 (1997).

[8] F.M. Yang, B. Nasunjilegal, J.L. Wang, H.Y. Pan, W.D. Qing, R.W. Zhao, B.P. Hu, Y.Z. Wang, G.C. Liu, H.S. Li, and J.M. Cadogan, J. Appl. Phys. **76**, 1971 (1994).

[9] B.P. Hu, G.C. Liu, Y.Z. Wang, B. Nasunjilegal, R.W. Zhao, F.M.

Yang, H.S. Li, and J.M. Cadogan, J. Phys.: Condens. Matter **6**, L197 (1994).
[10] V.R. Shah, G. Markandeyulu, K.V.S. Rama Rao, M.Q. Huang, K. Sirisha, and M.E. McHenry, J. Magn. Magn. Mater. **190**, 233 (1998).
[11] D. Yang, J.L. Wang, N. Tang, Y.P. Shen, and F.M. Yang, Appl. Phys. Lett. **74**, 4020 (1999).
[12] W.Q. Wang, J.L. Wang, D. Yang, N. Tang, F.M. Yang, G.H. Wu, and H.M. Jin, Chin. Phys. Lett. **18**, 969 (2001).
[13] V.G. Harris, Q. Huang, V.R. Shah, G. Markandeyulu, K.V.S. Rama Rao, M.Q. Huang, K. Sirisha, and M.E. McHenry, IEEE Trans. Magn. **35**, 3286 (1999).
[14] H.G. Pan, F.M. Yang, C.P. Chen, X.F. Han, N. Tang, J.F. Hu, J.L. Wang, R.W. Zhao, K.W. Zhou, and Q.D. Wang, J. Magn. Magn. Mater. **159**, 352 (1996).
[15] N.X. Chen, Phys. Rev. Lett. **64**, 1193 (1990).
[16] N.X. Chen and G.B. Ren, Phys. Rev. B **45**, 8177 (1992).
[17] N.X. Chen, X.J. Ge, W.Q. Zhang, and F.W. Zhu, Phys. Rev. B **57**, 14 203 (1998).
[18] C.D. Fuerst, F.E. Pinkerton, and J.F. Herbst, J. Magn. Magn. Mater. **129**, L115 (1994).
[19] F. Bolzoni, O. Moze, and L. Pareti, J. Appl. Phys. **62**, 615 (1987).
[20] H.S. Li, D. Courtois, and J.M. Cadogan, J. Appl. Phys. **79**, 4622 (1996).
[21] D. Courtois, H.S. Li, and J.M. Cadogan, Solid State Commun. **98**, 565 (1996).
[22] Y. Matsuura, S. Hirosawa, H. Yamamoto, S. Fujimura, and M. Sagawa, Appl. Phys. Lett. **46**, 308 (1985).
[23] O. Kalogirou, C. Sarafidis, M. Gjoka, T. Bakas, and M. Giannouri, J. Alloys Compd. **325**, 59 (2001).
[24] D. Givord, and R. Lemaire, IEEE Trans. Magn. **10**, 109 (1974).
[25] J.P. Gavigan, D. Givord, H.S. Li, and J. Voiron, Physica B **149**, 345 (1988).
[26] J.L. Wang, N. Tang, R.W. Zhao, F.M. Yang, and R.F. de Boer, J. Magn. Magn. Mater. **166**, 355 (1997).
[27] K.H.J. Buschow, *Ferromagnetic Materials*, edited by E.P. Wohlfarth and K.H.J. Buschow (North-Holland, Amsterdam, 1988), Vol. 4, p. 63.
[28] M. Jurczyk, G.K. Nicolaides, and K.V. Rao, J. Appl. Phys. **70**, 6110 (1991).
[29] Z.W. Li, X.Z. Zhou, and A.H. Morrish, Phys. Rev. B **41**, 8617 (1990).
[30] Z.W. Li, X.Z. Zhou, and A.H. Morrish, Phys. Rev. B **51**, 2891 (1995).
[31] Z.W. Li, and A.H. Morrish, Phys. Rev. B **55**, 3670 (1997).
[32] H.G. Pan, F.M. Yang, C.P. Chen, X.F. Han, N. Tang, and Q.D. Wang, J. Magn. Magn. Mater. **161**, 177 (1996).
[33] J.P. Perdew, J.A. Chevary, S.H. Vosko, K.A. Jackson, M.R. Pederson, D.J. Singh, and C. Fiolhais, Phys. Rev. B **46**, 6671 (1992).
[34] J.A. White and D.M. Bird, Phys. Rev. B **50**, 4954 (1994).
[35] W.Q. Zhang, Q. Xie, X.J. Ge, and N.X. Chen, J. Appl. Phys. **82**, 578 (1997).
[36] Y.M. Kang, N.X. Chen, and J. Shen, J. Magn. Magn. Mater. **256**, 381 (2003).
[37] N.X. Chen, J. Shen, and X.P. Su, J. Phys.: Condens. Matter **13**, 2727 (2001).
[38] Y.M. Kang, N.X. Chen, and J. Shen, J. Alloys Compd. **352**, 26 (2003).
[39] S.Q. Hao, N.X. Chen, and J. Shen, J. Alloys Compd. **343**, 53 (2002).
[40] S. Zhang and N.X. Chen, Phys. Rev. B **66**, 064106 (2002).
[41] Y. Liu, N.X. Chen, and Y.M. Kang, Mod. Phys. Lett. B **16**, 187 (2002).